

Correlated electrons in the presence of disorder

K. Byczuk,^{1,2} W. Hofstetter,³ U. Yu,⁴ and D. Vollhardt^{2,a}

¹ Institute of Theoretical Physics, University of Warsaw, ul. Hoża 69, 00-681 Warszawa, Poland

² Theoretical Physics III, Center for Electronic Correlations and Magnetism, Institute for Physics, University of Augsburg, 86135 Augsburg, Germany

³ Institut für Theoretische Physik, Johann Wolfgang Goethe-Universität, 60438 Frankfurt/Main, Germany

⁴ School of General Studies, Gwangju Institute of Science and Technology, Gwangju 500-712, Korea

Abstract. Several new aspects of the subtle interplay between electronic correlations and disorder are reviewed. First, the dynamical mean-field theory (DMFT) together with the geometrically averaged (“typical”) local density of states is employed to compute the ground state phase diagram of the Anderson-Hubbard model at half-filling. This non-perturbative approach is sensitive to Anderson localization on the one-particle level and hence can detect correlated metallic, Mott insulating and Anderson insulating phases and can also describe the competition between Anderson localization and antiferromagnetism. Second, we investigate the effect of binary alloy disorder on ferromagnetism in materials with f -electrons described by the periodic Anderson model. A drastic enhancement of the Curie temperature T_c caused by an increase of the local f -moments in the presence of disordered conduction electrons is discovered and explained.

1 Introduction

Electronic correlations are known to lead to a plethora of fascinating phenomena [1,2,3,4,5,6,7,8]. The same holds true for disorder in quantum systems [9,10,11,12,13,14,15,16,17]. Both limits, electronic correlations without disorder and disorder without electronic correlations, are notoriously difficult to treat since interactions lead to a highly complicated many-body problem, while disorder requires the application of statistical methods to average over the disorder. The simultaneous presence of interactions and disorder, often encountered in real materials, therefore implies an even more complex many-body problem [18,19,20,21,22,23,24,25,26,27,28,29,30] which is still far from understood. Namely, repulsive interactions and disorder are both driving forces behind metal-insulator transitions (MITs) connected with the localization and delocalization of particles. While the Coulomb interaction may trigger a Mott-Hubbard MIT [4,6,31], the scattering of non-interacting particles from randomly distributed impurities can lead to Anderson localization [9,32].

The exploration of phenomena which take place at intermediate or strong couplings, e.g., ferromagnetism and the Mott-Hubbard MIT with and without disorder are of particular interest. Here the recently developed dynamical mean-field theory (DMFT) [33,34,35,36,37,38,39,40,41] has proved to provide an excellent, comprehensive mean-field approximation, which may be employed for arbitrary values of the input parameters. For this reason the DMFT has been successfully applied in the investigation of electronic correlation effects in theoretical models and even real materials [41,42,43,44].

^a e-mail: dieter.vollhardt@physik.uni-augsburg.de

In this paper we review recent results on correlated electron systems in the presence of disorder obtained within the DMFT. In particular, we explore the low-temperature phase diagram of the Anderson-Hubbard model at half-filling, where disordered metallic, Anderson localized, and Mott insulating paramagnetic phases compete with antiferromagnetic long-range order. For comparison we then investigate the phase diagram of the simpler Falicov-Kimball model. Finally we discuss the influence of the band-splitting by binary alloy type disorder on properties of the periodic Anderson model. In particular, we show that alloy disorder not only leads to a non-monotonic changes of the Curie temperature T_c as a function of some control parameter, and even to an enhancement of T_c compared to the non-disordered case, but also to the formation of Mott or Kondo insulators at non-integer electron densities.

2 Correlated electron systems in the presence of disorder

The models investigated here are the Anderson-Hubbard model

$$H = \sum_{ij,\sigma} t_{ij} c_{i\sigma}^\dagger c_{j\sigma} + \sum_{i\sigma} \epsilon_i n_{i\sigma} + U \sum_i n_{i\uparrow} n_{i\downarrow}, \quad (1)$$

where t_{ij} is the hopping matrix element, U is the local Coulomb interaction, $c_{i\sigma}^\dagger$ is the fermionic creation operator for an electron with spin σ in Wannier state i , and $n_{i\sigma}$ is the particle number operator; and the Anderson-Falicov-Kimball model

$$H = \sum_{ij} t_{ij} c_i^\dagger c_j + \sum_i \epsilon_i c_i^\dagger c_i + U \sum_i f_i^\dagger f_i c_i^\dagger c_i, \quad (2)$$

where c_i^\dagger (f_i^\dagger) and c_i (f_i) are fermionic creation and annihilation operators for *mobile* (*immobile*) particles at a lattice site i . Furthermore, t_{ij} is the hopping amplitude for mobile particles between sites i and j , and U is the local interaction energy between mobile and immobile particles occupying the same site. The ionic energy ϵ_i in both models is a random, independent variable which describes the local, quenched disorder affecting the motion of the mobile particles.

The disorder part is modeled by a corresponding probability distribution function (PDF) $P(\epsilon_i)$. A model of disorder that we use is one with the continuous PDF

$$P(\epsilon_i) = \frac{\Theta(\frac{\Delta}{2} - |\epsilon_i|)}{\Delta}, \quad (3)$$

with Θ as the step function. The parameter Δ is then a measure of the disorder strength.

2.1 Dynamical mean-field theory with disorder

Dynamical mean-field theory is based on the observation that in the high-dimensional limit $d \rightarrow \infty$ (or equivalently $Z \rightarrow \infty$, where Z is the lattice coordination number) the self-energy $\Sigma_{ij}(\omega)$ as defined by the Dyson equation

$$G_{ij\sigma}(i\omega_n)^{-1} = G_{ij\sigma}^0(i\omega_n)^{-1} - \Sigma_{ij\sigma}(i\omega_n), \quad (4)$$

where i, j denote lattice sites and $\omega_n = (2n + 1)\pi/\beta$ are fermionic Matsubara frequencies, becomes diagonal in real-space [33,34]

$$\Sigma_{ij\sigma}(i\omega_n) = \Sigma_{i\sigma}(i\omega_n) \delta_{ij}, \quad (5)$$

provided the hopping amplitudes are scaled properly to ensure a balance of kinetic and interaction energy in this limit. For nearest-neighbour hopping on a hypercubic lattice this implies the scaling $t = t^*/\sqrt{2d} = t^*/\sqrt{Z}$. In a homogeneous system the self-energy is also site independent,

i.e., $\Sigma_{ij\sigma}(i\omega_n) = \Sigma_{\sigma}(i\omega_n) \delta_{ij}$, and is only a function of the energy. The DMFT approximation when applied to finite-dimensional systems neglects off-diagonal parts of the self-energy. In other words, the DMFT takes into account all temporal fluctuations but neglects spatial fluctuations between different lattice sites [41,43].

Here we present recent developments regarding the application of DMFT to correlated fermion systems with disorder. Within DMFT each correlated lattice site is mapped onto a single impurity, which is coupled to a dynamical mean-field bath describing the influence of all remaining lattice sites. This coupling is represented by the hybridization function $\eta_{i\sigma}(\omega)$, which needs to be determined self-consistently. The mapping is performed for all N_L lattice sites.

In the presence of disorder as given by a particular realization of onsite energies $\{\epsilon_1, \epsilon_2, \dots, \epsilon_{N_L}\}$ the total partition function can be written as a product of the N_L partition functions of the individual impurities

$$Z = \prod_i Z_i = \prod_i \exp \left(\sum_{\sigma\omega_n} \ln [i\omega_n + \mu - \epsilon_i - \eta_{i\sigma}(\omega_n) - \Sigma_{i\sigma}(\omega_n)] \right). \quad (6)$$

where the hybridization function $\eta_{i\sigma}(\omega_n)$ formally represents a site- and time-dependent one-particle potential. The unitary time evolution due to this potential can therefore be described by a local, time-dependent evolution operator [45,46]

$$U[\eta_{i\sigma}] = T_{\tau} e^{-\int_0^{\beta} d\tau \int_0^{\beta} d\tau' c_{i\sigma}^{\dagger}(\tau) \eta_{i\sigma}(\tau - \tau') c_{i\sigma}(\tau')}, \quad (7)$$

where the interaction representation has been used, T_{τ} is the time ordering operator, and $c_{i\sigma}(\tau)$ evolves according to the atomic part H_i^{loc} of the Hamiltonians (1) or (2) in imaginary Matsubara time $\tau \in (0, \beta)$. We write the partition function (6) as a trace

$$Z = Z[\eta_{i\sigma}] = \prod_{i=1}^{N_L} \text{Tr} \left[e^{-\beta(H_i^{\text{loc}} - \mu N_i^{\text{loc}})} U[\eta_{i\sigma}] \right], \quad (8)$$

where N_i^{loc} is the local particle number operator.

For a given dynamical mean-field $\eta_{i\sigma}(\omega_n)$ the local one-particle Green function $G_{ii\sigma}(\omega_n)$ is then determined from Eq. (8) by taking a functional logarithmic derivative of the partition function (8) with respect to $\eta_{i\sigma}(\omega_n)$

$$G_{ii\sigma}(\omega_n) = -\frac{\partial \ln Z[\eta_{i\sigma}]}{\partial \eta_{i\sigma}(\omega_n)}. \quad (9)$$

We thus obtain the local Dyson equations

$$\Sigma_{i\sigma}(\omega_n) = i\omega_n + \mu - \epsilon_i - \eta_{i\sigma}(\omega_n) - \frac{1}{G_{ii\sigma}(\omega_n)}, \quad (10)$$

for each of the N_L lattice sites. Eqs. (4, 5, 8, 9, and 10) constitute a closed set of self-consistency relations. The solution of these yields an approximate solution of the Hamiltonian (1) or (2) for a given disorder realization.

2.2 Disorder averages

Solving Eqs. (4, 5, 8, 9, and 10) rigorously is in general only possible for small N_L , since it requires an exact evaluation of the time evolution operator (7) at each impurity site. However, in disordered systems one is mostly interested in the thermodynamic limit $N_L \rightarrow \infty$ where localized and extended states can be distinguished reliably. Here one faces a typical trade-off situation in computational physics. A solution to this problem is obtained by a *statistical* approach in combination with DMFT, as applied by us [47,48,49] and outlined in the following.

Given a particular disorder realization $\{\epsilon_1, \epsilon_2, \dots, \epsilon_{N_L}\}$ one could in principle obtain from the solution of the DMFT equations a set of realization-dependent local densities of states (LDOS)

$$A_{i\sigma}(\omega) = -\frac{1}{\pi} \text{Im} G_{ii\sigma}(\omega_n \rightarrow \omega + i0^+). \quad (11)$$

Usually, however, one is interested in physical information about a system that does not depend on a particular disorder realization. This makes a statistical interpretation of the solutions of Eqs. (4, 5, 8, 9, and 10) necessary.

A common approach for systems in the thermodynamic limit $N_L \rightarrow \infty$ is to take the arithmetic average of the LDOS $A_{i\sigma}(\omega)$ over many realizations of the disorder, i.e.,

$$\langle A_{i\sigma}(\omega) \rangle = \int \prod_{j=1}^{N_L} d\epsilon_j P(\epsilon_i) A_{i\sigma}(\omega; \{\epsilon_1, \dots, \epsilon_{N_L}\}). \quad (12)$$

By performing the arithmetic average one restores the translational invariance in the description of the disordered system, i.e. the average $A_\sigma(\omega)_{\text{arith}} = \langle A_{i\sigma}(\omega) \rangle$ is the same for all lattice sites. However, this only leads to meaningful results if both the system and the physical observable under study are self-averaging.

An example of a *non*-self-averaging system is a disordered system at the Anderson localization transition [9]. This implies that during the time evolution, a particle cannot explore the full phase space, i.e., cannot probe all possible random distributions. In such a case the arithmetic average (12) is inadequate. Here one is faced with the question concerning the proper statistical description of such a system.

As pointed out by Anderson [9], the solution to this problem is to investigate the full PDF for a given physical observable $P[A_{i\sigma}(\omega)]$ and to identify its most probable value – the “typical” value $A_\sigma(\omega)_{\text{typ}}$ – i.e. the value where the PDF $P[A_{i\sigma}(\omega)]$ has a global maximum. This typical value will be the same on each lattice site and represent typical properties of the system. By considering $A_\sigma(\omega)_{\text{typ}}$ one thus restores translational invariance in the description of a disordered system. Using photoemission spectroscopy one could, in principle, experimentally probe the LDOS at different lattice sites and measure its most probable value. We note that if sample-to-sample fluctuations are small, the typical value $A_\sigma(\omega)_{\text{typ}}$ coincides with the arithmetic average $A_\sigma(\omega)_{\text{arith}}$. On the other hand, in a non-self-averaging system the PDF can be strongly asymmetric, with a long tail, in which case the typical value $A_\sigma(\omega)_{\text{typ}}$ would strongly differ from $A_\sigma(\omega)_{\text{arith}}$. In this case the arithmetic mean is strongly biased by rare fluctuations and hence does not represent the typical property of such a system.

Calculating the full probability distribution of the LDOS typically requires the inclusion of a large number of impurity sites, which for interacting systems is hard to achieve computationally, although there have been recent successful attempts in this direction [50]. A more efficient approach is based on identifying a generalized average which yields the best approximation to the typical value. Among several different means the *geometric* mean

$$A_\sigma(\omega)_{\text{geom}} = \exp[\langle \ln A_{i\sigma}(\omega) \rangle], \quad (13)$$

turns out to be very convenient to describe Anderson localization, where it represents a good approximation to the typical value:

$$A_\sigma(\omega)_{\text{typ}} \approx A_\sigma(\omega)_{\text{geom}}. \quad (14)$$

Here $\langle F(\epsilon_i) \rangle = \int \prod_i d\epsilon_i \mathcal{P}(\epsilon_i) F(\epsilon_i)$ denotes the arithmetic mean of the function $F(\epsilon_i)$. It is easy to see that in the special case when $P[A_{i\sigma}(\omega)]$ is a log-normal distribution the relation $A_\sigma(\omega)_{\text{typ}} = A_\sigma(\omega)_{\text{geom}}$ holds exactly. For the noninteracting Anderson disorder model it was shown that $A_\sigma(\omega)_{\text{geom}}$ vanishes at a critical strength of the disorder, thereby providing an explicit criterion for Anderson localization [9,51,52,53,54]. It should be noted that the geometrically averaged LDOS only includes extended states, i.e., it is finite only if the spectrum is continuous. Hence it is not normalized to unity.

By using the geometrically averaged LDOS one arrives at a translational invariant description of the disordered system. This allows one to solve the DMFT equations in the thermodynamic limit as will be demonstrated in the next section. The problem of finite-size effects is then absent, and the main limitation is due to the finite accuracy of the impurity solver.

2.3 Self-consistency conditions of the DMFT with disorder

Once the geometrically averaged local spectrum has been obtained, the corresponding local Green function is given by

$$G_{\sigma}(\omega_n)_{\text{geom}} = \int d\omega \frac{A_{\sigma}(\omega)_{\text{geom}}}{i\omega_n - \omega}, \quad (15)$$

which allows one to recast the DMFT self-consistency condition (10) into the following translationally invariant form

$$\Sigma_{\sigma}(\omega_n) = i\omega_n + \mu - \eta_{\sigma}(\omega_n) - \frac{1}{G_{\sigma}(\omega_n)_{\text{geom}}}. \quad (16)$$

where a vanishing average on-site energy $\langle \epsilon_i \rangle = 0$ has been assumed, which holds in particular for the box-shape PDF. On the other hand, Fourier transformation of the lattice Dyson equation (4) yields

$$G_{\sigma}(\omega_n)_{\text{geom}} = \int dz \frac{N_0(z)}{\omega_n - z + \mu - \Sigma_{\sigma}(\omega_n)}, \quad (17)$$

which closes the set of DMFT self-consistency relations. We note that the self-consistency equation (17) gives the same geometrically averaged Green function as that obtained from (15). Here $N_0(z)$ is the density of states for a non-interacting lattice system without disorder.

The above discussion shows that by taking the geometric average of the LDOS one i) restores translational invariance and ii) can directly address the thermodynamic limit. The DMFT calculations are thus no longer affected by finite-size effects.

For the description of antiferromagnetic long-range order the self-consistency relations need to be modified. In this case one introduces two sublattices $s = A$ or B , and calculates the two corresponding local Green functions $G_{ii\sigma s}(\omega_n)$, which are no longer identical. Geometric averaging of the LDOS given by Eq. (11) yields $A_{\sigma s}(\omega)_{\text{geom}} = \exp[\langle \ln A_{i\sigma s}(\omega) \rangle]$. The local Green function is then again obtained from the Hilbert transform (15), and the self-energy $\Sigma_{\sigma s}(\omega)$ from the local Dyson equation Eq. (16). Finally, the self-consistent DMFT equations are closed by the Hilbert transform of the Green function on a bipartite lattice:

$$G_{\sigma s}(\omega_n)_{\text{geom}} = \int dz \frac{N_0(z)}{\left[\omega_n - \Sigma_{\sigma s}(\omega_n) - \frac{z^2}{\omega - \Sigma_{\sigma \bar{s}}(\omega_n)} \right]} \quad (18)$$

where \bar{s} denotes the sublattice opposite to s [55,41].

As a concluding remark regarding the formalism we note that replacing the geometric mean by arithmetic averaging would lead to a description of disorder effects on the CPA level only, which would not allow to detect Anderson localization. We also point out that in the presence of disorder the typical LDOS $A_{\sigma}(\omega)_{\text{geom}}$ is not normalized to unity. This means that $A_{\sigma}(\omega)_{\text{geom}}$ only describes extended states, i.e. the continuum part of the spectrum. The contribution of localized states to the LDOS is not captured by DMFT with geometric averaging. Therefore, this approach cannot describe spectral properties of the Anderson-insulator phase.

3 Phase transitions in the disordered Hubbard model

3.1 Characterization of phases

Our goal is to determine the ground-state phase diagram of the Anderson-Hubbard Hamiltonian (1). In order to characterize the different relevant phases, we compute several physical observables:

1. the LDOS $A_{\sigma s}(\omega)_{\text{geom}}$ for a given sublattice s and spin direction σ ;
2. the total DOS for a given sublattice s at the Fermi level ($\omega = 0$) with $N_s(0)_{\text{geom}} \equiv \sum_{\sigma} A_{\sigma s}(\omega = 0)_{\text{geom}}$;
3. the staggered magnetization $m_{\text{AF}}^{\text{geom}} = |n_{\uparrow A}^{\text{geom}} - n_{\uparrow B}^{\text{geom}}|$, where $n_{\sigma s}^{\text{geom}} = \int_{-\infty}^0 d\omega A_{\sigma s}(\omega)_{\text{geom}}$ is the local particle density on sublattice s .

The possible phases of the Anderson-Hubbard model can then be classified as follows: The systems is a

- paramagnetic metal if $N_s^{\text{geom}}(0) \neq 0$ and $m_{\text{AF}}^{\text{geom}} = 0$;
- AF metal if $N_s^{\text{geom}}(0) \neq 0$ and $m_{\text{AF}}^{\text{geom}} \neq 0$;
- AF insulator if $N_s^{\text{geom}}(0) = 0$ and $m_{\text{AF}}^{\text{geom}} \neq 0$ but $N_s^{\text{geom}}(\omega) \neq 0$ for some $\omega \neq 0$ (in fact, the last condition is already implied by $m_{\text{AF}}^{\text{geom}} \neq 0$);
- paramagnetic Anderson-Mott insulator if $N_s^{\text{geom}}(\omega) = 0$ for all ω .

In the following we consider the Anderson-Hubbard model at half-filling and determine its paramagnetic as well as magnetic phases at $T = 0$ using the formalism described above [47,49]. For computational convenience, we choose a model DOS, $N_0(\epsilon) = 2\sqrt{D^2 - \epsilon^2}/\pi D^2$, with bandwidth $W = 2D$, and set $W = 1$ in the following. For this DOS and for a bipartite lattice the local Green function and the hybridization function are connected by the simple algebraic relation $\eta_{\sigma s}(\omega)_{\text{geom}} = D^2 G_{\sigma s}(\omega)_{\text{geom}}/4$. [41]

The resulting DMFT equations are solved at zero temperature by the numerical renormalization group technique [56,57,58], which allows us to solve the effective Anderson impurity problem and thus to determine the LDOS and its averages.

3.2 Mott-Hubbard transition vs. Anderson localization

In Fig. 1 we show the paramagnetic ground-state phase diagram of the Anderson-Hubbard model at half-filling obtained by the DMFT formalism detailed above. Two different quantum phase transitions can be observed: a Mott-Hubbard MIT for weak disorder Δ , and an Anderson MIT for weak interaction U . In the following we will discuss these transitions as well as the properties of the two different insulating phases and of the correlated, disordered metallic phase. Since these phases are all paramagnetic the spin index will be omitted in this section.

(i) *Disordered, metallic phase*: The correlated, disordered metal is characterized by a finite value of the spectral density at the Fermi level, $A(\omega = 0)_{\text{geom}} \neq 0$.

(ii) *Mott-Hubbard MIT*: For weak to intermediate disorder strength a sharp transition between a correlated metal and a gapped Mott insulator occurs at a critical value of U . Two transition lines are found depending on whether the MIT is approached from the metallic [$\Delta_{c2}^{MH}(U)$, full dots in Fig. 1] or from the insulating side [$\Delta_{c1}^{MH}(U)$, open dots in Fig. 1]. The curves $\Delta_{c1}^{MH}(U)$ and $\Delta_{c2}^{MH}(U)$ in Fig. 1 are seen to have positive slope. This is due to the disorder-induced increase of spectral weight at the Fermi level which in turn requires a stronger interaction to open the correlation gap. As a result, close to the hysteretic region an increase of disorder will drive the system from the Mott insulator *back* into the metallic phase or, equivalently, protect the metal from becoming a Mott insulator.

The transition lines $\Delta_{c1}^{MH}(U)$ and $\Delta_{c2}^{MH}(U)$ terminate at a single critical point around $\Delta \approx 1.8$, cf. Fig. 1. For stronger disorder ($\Delta > 1.8$) we observe a smooth crossover rather than a sharp metal-insulator transition.

(iii) *Anderson MIT*: Next to the metallic phase and the crossover regime an Anderson insulator is found where the LDOS of the extended states, as obtained by geometric averaging, vanishes completely (see Fig. 1). The associated critical disorder strength $\Delta_c^A(U)$ at the Anderson MIT has a non-monotonic behaviour: while it first increases as a function of interaction in the metallic regime, it decreases again in the crossover regime. In the former case, an increase of interaction strength leads to re-entrant transition from the Anderson insulator into the correlated metal, where electronic correlations prevent quasiparticles from localization by elastic impurity scattering.

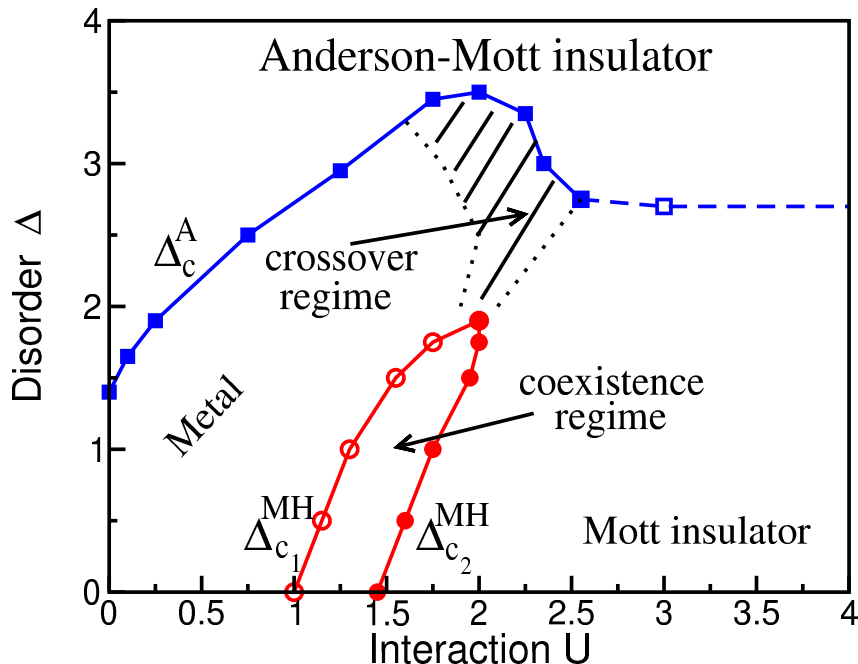


Fig. 1. Paramagnetic ground-state phase diagram of the Anderson–Hubbard model at half-filling obtained by DMFT with the typical local density of states [67].

(iv) *Anderson-Mott insulator*: We note that the Mott insulator (with a finite correlation gap in the single-particle spectrum) is rigorously defined only in the pure system ($\Delta = 0$), while the gapless Anderson insulator phase arises only for non-interacting systems ($U = 0$) with sufficiently strong disorder $\Delta > \Delta_c^A(0)$. In the simultaneous presence of finite interactions and disorder it is no longer possible to strictly distinguish these two phases. However, as long as the LDOS shows the characteristic Hubbard subbands the system may be termed a *disordered Mott insulator*. With increasing disorder Δ the spectral weight of the Hubbard subbands vanishes and the system can be considered a *correlated Anderson insulator*. The (crossover) boundary between these two types of insulators is marked by a dashed line in Fig. 1. Our DMFT results obtained here indeed show that the paramagnetic Mott and Anderson insulators are continuously connected. Hence, by changing U and Δ it is possible to move from one insulating state to another one without entering a metallic phase. This single connected, insulating phase is therefore termed the *Anderson-Mott insulator*.

3.3 Competition between Anderson localization and antiferromagnetism

In the previous section we have neglected antiferromagnetic ordering, which generically occurs at low temperatures on non-frustrated lattices and in the absence of disorder. Several fundamental questions arise: (i) How do local interactions influence a non-interacting, Anderson localized system at half-filling? (ii) How does an antiferromagnetic (AF) insulator at half-filling respond to disorder which in the absence of interactions would lead to an Anderson localized state? (iii) Can Slater and Heisenberg antiferromagnets be distinguished by their response to disorder? Here we provide answers to these questions by calculating the zero temperature, magnetic phase diagram of the disordered Hubbard model at half-filling using DMFT together with a geometric average over the disorder and allowing for a spin-dependence of the DOS [49].

Our results are shown in Fig. 2. The response of the system to disorder is found to be qualitatively different depending on whether the interaction U is weak or strong. At strong interactions, $U/W > 1$, only two phases exist, an AF insulating phase at weak disorder, $\Delta/W < 2.5$, and a paramagnetic Anderson-Mott insulator at strong disorder, $\Delta/W > 2.5$. The local

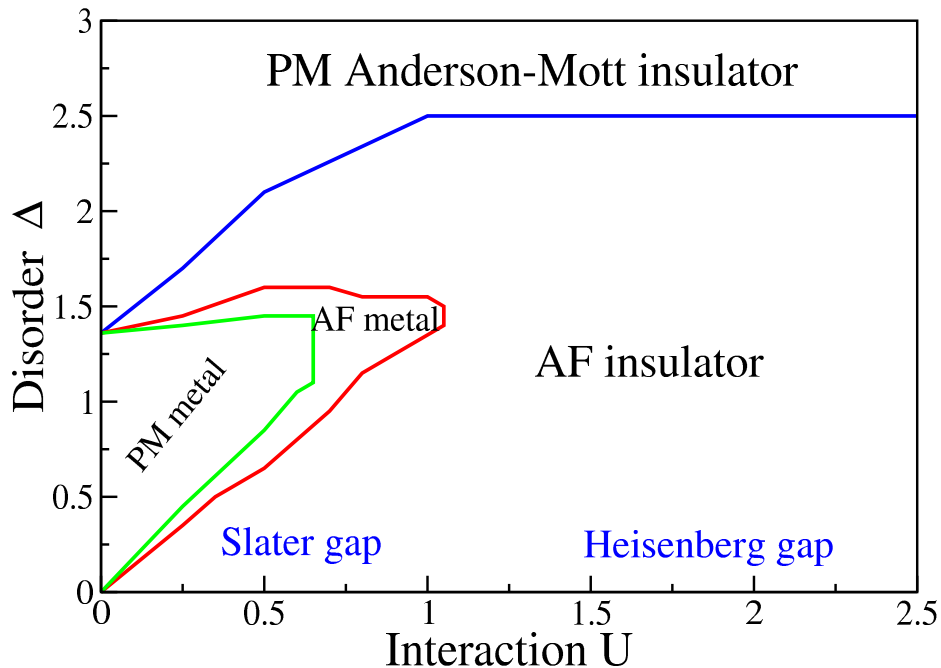


Fig. 2. Magnetic ground-state phase diagram of the Anderson-Hubbard model at half-filling as obtained by DMFT with a spin resolved, geometrically averaged local DOS (see text) [49].

DOS and the staggered magnetization both decrease gradually as the disorder Δ increases and vanish at the phase boundary, indicating that the associated quantum phase transition is continuous. On the other hand, a richer structure of the phase diagram is found for weak interactions, $U/W < 1$, (Fig. 2). In particular, for weak disorder a *paramagnetic* metallic phase is stable. It is separated from the AF insulator at large U by a narrow region of an *AF metallic* phase. The AF metal is characterized by long-range order in the absence of a gap, which is due to a redistribution of spectral weight induced by disorder [49].

In the pure system without disorder, the AF insulating phase can be characterized by two limiting regimes: a Slater antiferromagnet with a small gap at $U/W < 1$ and a Heisenberg regime with large gap at $U/W > 1$. These limits can be addressed by perturbation expansions in U and $1/U$ around the symmetry broken state of the Hubbard and the corresponding Heisenberg model, respectively. Our results for m_{AF} confirm that even in the presence of disorder there is no sharp transition between these limits, in agreement with earlier studies [59]. This may be attributed to the fact that both the Slater and the Heisenberg regime are characterized by the same order parameter. However, from our results (Fig. 2) it is evident that the two limits *can* be distinguished by their overall response to disorder. Namely, the reentrance of metallic antiferromagnetism at $\Delta/W > 1$ occurs only within the Slater AF insulating phase.

Let us finally remark that a disordered AF metallic phase is also obtained by DMFT combined with arithmetic averaging [55,60]. This approach however predicts that both the paramagnetic and the AF metal remain stable for arbitrarily strong disorder, which is clearly incorrect and closely related to the failure of CPA to capture disorder-induced localization. Only a computational approach which is sensitive to Anderson localization, such as the DMFT with geometrically averaged local DOS employed here, is able to detect already on the one-particle level the suppression of the metallic phase for $\Delta/W > 1.5$ and the appearance of the paramagnetic Anderson-Mott insulator at large disorder Δ .

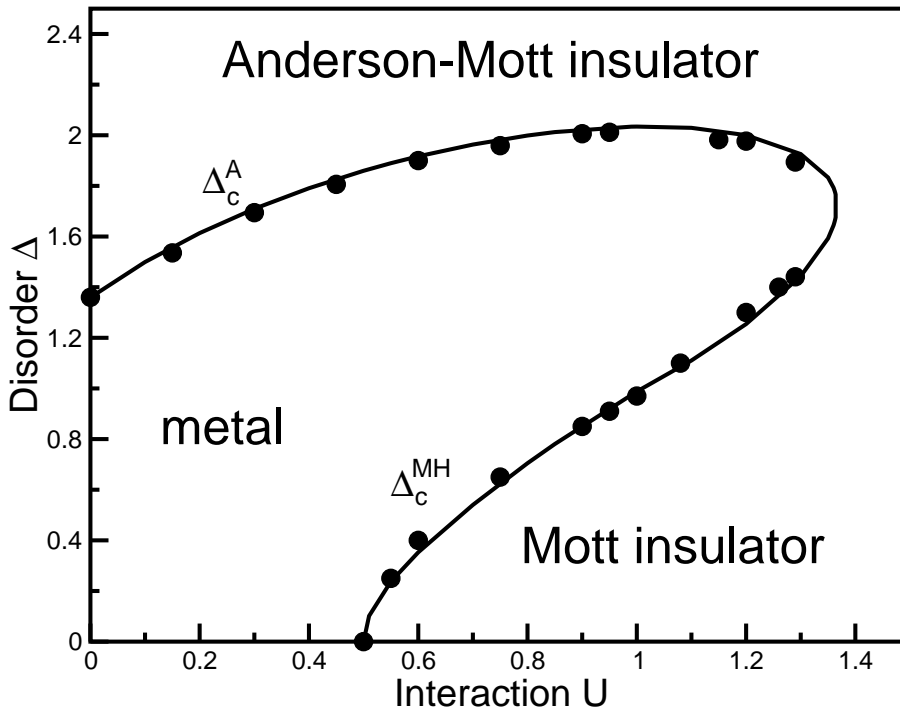


Fig. 3. Ground-state phase diagram of the Falicov-Kimball model at half-filling with disorder as obtained by the DMFT with geometric average [48]. Dots represent the numerical solution of the DMFT equations. The solid line was obtained analytically by the linearized DMFT.

4 Metal-insulator transitions in the disordered Falicov-Kimball model

We now apply the DMFT with geometric average over the disorder to the disordered Falicov-Kimball model at half-filling [48]. The non-interacting DOS for mobile particles and other physical parameters are the same as in the previous section. However, the DMFT equations are now solved differently: since in this case the functional integrals are Gaussian they are calculated analytically, and only the self-consistency loops are computed numerically.

4.1 Ground-state phase diagram

In the half-filled case the ground-state properties of the Falicov-Kimball model are determined by states in the center of the band, i.e., at $\omega = 0$. The ground-state phase diagram is shown in Fig. 3. In the presence of disorder the metallic phase is seen to be more extended than in the pure case. Namely, while for $\Delta = 0$ the (continuous) Mott-Hubbard MIT occurs at $U_c = W/2$, the presence of disorder shifts the transition to larger values of U : the phase boundary between the metal and the Mott insulator, $\Delta_c^{MH}(U)$ in Fig. 3 lies between $0 \leq \Delta \lesssim 1.70W$ and $W/2 \leq U \lesssim 1.36W$. By contrast, the Anderson MIT, which is also continuous, takes place along the phase boundary $\Delta_c^A(U)$ (see Fig. 3). Again the critical disorder strength increases for increasing U and extends between $0 < U \lesssim 1.36W$ and $eW/2 \leq \Delta \lesssim 2.03W$, where $e \approx 2.718$ is Euler's constant. Obviously the interaction impedes the localization of particles due to the scattering at the impurities. For large values of U and Δ there is no metallic phase.

The DMFT results shown here confirm that in the disordered Falicov-Kimball model the Mott insulator and the Anderson insulator are continuously connected. Hence, by changing U and Δ it is possible to move from one type of insulator to the other without having to cross a metallic phase. This scenario is supported by the fact that the Anderson MIT ($U = 0$) and the Mott-Hubbard MIT ($\Delta = 0$) are not associated with the breaking of a symmetry.

4.2 Linearized dynamical mean-field theory

In the vicinity of the MIT the linearized DMFT [52,61] may be employed to calculate the transition line analytically. Due to the symmetry properties of $A_{\text{geom}}(\omega)$ one finds $G(0) = -i\pi A_{\text{geom}}(0)$ at the band center, i.e., $G(0)$ is purely imaginary. The DMFT self-consistency then implies that the hybridization function obeys $\eta(0) = -i\pi W^2 A_{\text{geom}}(0)/16$.

Iteration of the DMFT equations leads to

$$A_i^{(n+1)}(0) = \frac{W^2}{16} A_{\text{geom}}^{(n)}(0) \mathcal{Y}(\epsilon_i), \quad (19)$$

where

$$\mathcal{Y}(\epsilon_i) = \frac{\epsilon_i^2 + \left(\frac{U}{2}\right)^2}{\left[\epsilon_i^2 - \left(\frac{U}{2}\right)^2\right]^2}. \quad (20)$$

After the geometric average the recursive relations in the linearized DMFT are given by

$$A_{\text{geom}}^{(n+1)}(0) = A_{\text{geom}}^{(n)}(0) \frac{W^2}{16} \exp \left[\frac{1}{\Delta} \int_{-\Delta/2}^{\Delta/2} d\epsilon \ln \mathcal{Y}(\epsilon) \right]. \quad (21)$$

While in the metallic phase the quantity $A_{\text{geom}}^{(n)}(0)$ increases upon recursion, i.e., $A_{\text{geom}}^{(n+1)}(0) > A_{\text{geom}}^{(n)}(0)$, it decreases in the insulating phase. Therefore, at the boundary between the metallic and the insulating solution the recursion does not depend on n , i.e., $A_{\alpha}^{(n+1)}(0) = A_{\alpha}^{(n)}(0)$. This condition directly determines the MIT transition at $\Delta = \Delta(U)$:

$$1 = \frac{W^2}{16} \exp \left[\frac{1}{\Delta} \int_{-\Delta/2}^{\Delta/2} d\epsilon \ln \mathcal{Y}(\epsilon) \right] \equiv \frac{W^2}{16} \exp [I_{\text{geom}}(U, \Delta)]. \quad (22)$$

The integral is evaluated analytically with the result

$$I_{\text{geom}}(U, \Delta) = 2 + \ln \left[\left(\frac{U}{2}\right)^2 + \left(\frac{\Delta}{2}\right)^2 \right] - 2 \ln \left[\left(\frac{U}{2}\right)^2 - \left(\frac{\Delta}{2}\right)^2 \right] + \frac{2U}{\Delta} \left[\arctan \left(\frac{\Delta}{U}\right) - \ln \left| \frac{\Delta+U}{\Delta-U} \right| \right]. \quad (23)$$

The solution of Eq. (22), shown as a solid line in Fig. 3, is found to agree very well with the numerical result. For weak interactions U the critical disorder strength obtained from (22) increases linearly in U , i.e., $\Delta(U) \approx W\epsilon/2 + \pi U/2$, since the total bandwidth increases linearly with U . For weak disorder Δ the solution of Eq. (22) is given by $\Delta(U) \approx \sqrt{U^2 - (W/2)^2}$. This agrees with the result obtained from the arithmetic average [48], which is not surprising since for weak disorder both averages must give the same result.

5 Ferromagnetism and Kondo insulator behavior in the disordered periodic Anderson model

In Secs. III and IV we discussed the results obtained for the Mott and Anderson MITs in correlated electron systems where the disorder had a continuous distribution, i.e., the probability distribution function of the local atomic energies was given by a piecewise continuous function of the energy (“box disorder”). However, to model binary-alloy systems a bimodal probability distribution function is more appropriate. This type of disorder also leads to a diffusive motion of the electrons, and even to Anderson localization, as the disorder with continuously distributed

energies [50]. But, for sufficiently high disorder strength the binary alloy disorder causes in addition a splitting of the band (“alloy band-splitting”) in arbitrary dimensions. It is therefore important to understand how the opening of two different kinds of gaps – the gap due to the alloy band-splitting and the Mott gap – affects the properties of the system.

In the following we employ the DMFT with arithmetic averaging over the binary alloy disorder [55]. As discussed earlier, this approach cannot detect Anderson localization on the level of one-particle quantities such as the density of states. However, for a discussion of the effect of band splitting on the correlated electrons such an approach is quite appropriate. In any case, the investigation can be extended to include the geometric average [50].

In the case of the one-band Hubbard model with the binary-alloy disorder we found the following interesting effects: (i) for band filling ν commensurate with the concentration of alloy atoms x , i.e., for $\nu = x$ or $1 + x$, the Mott-Hubbard MIT can take place for non-integer values of ν , (ii) depending on the ratio between the Mott gap and the alloy gap the correlated alloy insulator at non-integer filling can be classified either as a *Mott-alloy insulator* (when the Mott gap is smaller than the alloy gap) or as a *charge-transfer alloy insulator* (when the Mott gap is larger than the alloy gap), (iii) at low filling and for particular values of the alloy concentration the Curie temperature increases in comparison with the pure system under the same conditions. We now discuss our results for an analogous problem, namely, the effect of binary alloy disorder on the properties of correlated f electrons which hybridize with a non-interacting band of conduction electrons, as described by the periodic Anderson model (PAM).

5.1 Periodic Anderson model with binary alloy disorder

The Hamiltonian of the PAM with binary alloy disorder is given by

$$H_{\text{PAM}} = \sum_{i,j\sigma} t_{ij} c_{i\sigma}^\dagger c_{j\sigma} + \sum_{i\sigma} \left(\varepsilon_i^f f_{i\sigma}^\dagger f_{i\sigma} + \varepsilon_i^c c_{i\sigma}^\dagger c_{i\sigma} \right) + \sum_{i\sigma} \left(V c_{i\sigma}^\dagger f_{i\sigma} + V^* f_{i\sigma}^\dagger c_{i\sigma} \right) + U \sum_i n_{i\uparrow}^f n_{i\downarrow}^f. \quad (24)$$

Here $c_{i\sigma}^\dagger$ ($c_{i\sigma}$) and $f_{i\sigma}^\dagger$ ($f_{i\sigma}$) are creation (annihilation) operators of conduction (c) and localized (f) electrons with spin σ at a lattice site i . The microscopic parameters in this model are the hopping amplitude t_{ij} of the c -electrons, the random on-site energies ε_i^f and ε_i^c , and V , the local hybridization between f - and c -electrons. The Coulomb interaction U acts only between f -electrons on the same site. The alloy is modeled by a bimodal probability distribution function

$$P(y_i) = x\delta(y_i - y_0) + (1 - x)\delta(y_i - y_0 - \Delta^y), \quad (25)$$

where $y_i = \varepsilon_i^c$, ε_i^f are independent, random variables with reference values $y_0 = \varepsilon_0^c$, ε_0^f . The alloy concentration is characterized by the parameter x and the difference between the atomic energies of the alloy components by $\Delta^y = \Delta^c$, Δ^f , respectively.

5.2 Alloy-band splitting of non-interacting electrons

The PAM [Eq. (24)] is solved within the DMFT by mapping it onto a corresponding single-impurity problem. The arithmetically averaged local Green functions can be written in matrix form as

$$\mathbf{G}_\sigma^{\text{loc}}(\tau; \{y_i\}) = - \begin{pmatrix} \langle T_\tau f_\sigma(\tau) f_\sigma^\dagger(0) \rangle & \langle T_\tau f_\sigma(\tau) c_\sigma^\dagger(0) \rangle \\ \langle T_\tau c_\sigma(\tau) f_\sigma^\dagger(0) \rangle & \langle T_\tau c_\sigma(\tau) c_\sigma^\dagger(0) \rangle \end{pmatrix}.$$

They are expressed in terms of local self-energies which appear in the \mathbf{k} -integrated Dyson equation $\Sigma_{\sigma n} = \mathcal{G}_{\sigma n}^{-1} - \mathbf{G}_{\sigma n}$. Here $\mathcal{G}_{\sigma n}$ is the matrix of local Green functions of the non-interacting bath electrons, with

$$\mathcal{G}_{\sigma n}^{-1} = \begin{pmatrix} i\omega_n + \mu - \varepsilon_0^f & V^* \\ V & i\omega_n + \mu - \varepsilon_0^c - \eta_{\sigma n} \end{pmatrix}.$$

To understand the effect of the disorder on the physics described by the PAM it is instructive to investigate the case $U = 0$ first. For $U = 0$ the corresponding impurity problem is quadratic and the functional integrals can be performed analytically. However, in the case of a two-band system like the PAM, where f - and c -electrons hybridize, the situation is more complicated than in the one-band case discussed earlier, since disorder affects a hybridized two-band system in several nontrivial ways.

We now consider the case where the alloy disorder acts either on the c -electrons or the f -electrons, respectively. In the case of c -electron disorder the diagonal local Green functions are given by

$$\begin{aligned} G_{\sigma n}^{cc} &= \frac{x}{(\mathcal{G}_{\sigma n}^{cc})^{-1} - |V|^2 \mathcal{G}_{\sigma n}^{ff}} + \frac{1-x}{(\mathcal{G}_{\sigma n}^{cc})^{-1} - |V|^2 \mathcal{G}_{\sigma n}^{ff} - \Delta^c} \\ G_{\sigma n}^{ff} &= \frac{x}{(\mathcal{G}_{\sigma n}^{ff})^{-1} - |V|^2 \mathcal{G}_{\sigma n}^{cc}} + \frac{1-x}{(\mathcal{G}_{\sigma n}^{ff})^{-1} - \frac{|V|^2}{(\mathcal{G}_{\sigma n}^{cc})^{-1} - \Delta^c}}. \end{aligned} \quad (26)$$

The case of f -electron disorder is obtained by exchanging $f \leftrightarrow c$ in (26). Alloy disorder acting only on the c -electrons leads to a band splitting of the conduction electrons for large enough energy splitting Δ^c . As in the single-band model each alloy subband then contains $2xN_L$ and $2(1-x)N_L$ states, respectively. The c -electron alloy subbands are separated by the energy Δ^c . One might expect that, due to the hybridization of c - and f -electrons, a similar effect would also occur in the f -electron subsystem. However, this is not the case. Namely, as seen from (26) a hybridization between the f -states and the $2(1-x)N_L$ states from the upper alloy c -electron subband is no longer possible for $\Delta^c \rightarrow \infty$. In this limit a (non-dispersive) f -level with $2(1-x)N_L$ states appears at the energy ε_0^f , in analogy with the case without hybridization ($V = 0$). Consequently, for infinitely strong binary alloy disorder in the c -electron system $2(1-x)N_L$ f -electron states become localized for arbitrary but finite values of V . So for $\Delta^c \rightarrow \infty$ only $2(1-x)N_L$ c -electron states, rather than $4(1-x)N_L$ states, are split off from the spectrum and are shifted to high energies. We note that, although the band splitting scheme is different from the single-band model, the alloy with hybridized c - and f -electrons can still be a band insulator for total densities different from integer values (2 or 4). A schematic plot in Fig. 4 shows the projected density of states, $N^b(\omega) = -\text{Im} \sum_{\sigma} G_{\sigma}^{bb}(\omega)/\pi$, where $b = c$ or f , for a system without [panel (a)] and with [panel (b)] disorder. An analogous analysis of f -electron disorder shows that in this case, at large Δ^f , the f -electron band is split into alloy subbands. Hybridization between the $2(1-x)N_L$ states from the upper alloy f -band and the c -electrons is again prevented when $\Delta^f \rightarrow \infty$. Therefore, the corresponding fraction of the c -electron band is unchanged, i.e., remains at the same energies as in the non-disordered case. We thus see that even in the absence of interactions binary alloy disorder affects a hybridized two-band system and a single-band system in quite different ways.

5.3 Kondo-insulator of interacting electrons at fractional filling

In analogy to our findings for the Hubbard model with binary alloy disorder [62,63] an opening of a correlation gap, obtained by increasing the alloy band splitting Δ^c , is found for the PAM [64]; see Fig. 5. This is caused by the splitting of the c -electron band due to binary alloy disorder and the correlations between the f -electrons. Namely, when the energy splitting Δ^c is much larger than the width of the c -electron band the total number of available low-energy states is reduced from $4N_L$ to $[4 - 2(1-x)]N_L = 2(1+x)N_L$, whereby the filling effectively increases by a factor of $4/[2(1+x)]$, such that $n_{\text{tot}}^{\text{eff}} = 2n_{\text{tot}}/(1+x)$, if $n_{\text{tot}} < 2(1+x)$. For the filling $n_{\text{tot}} = 1.3$ studied in Fig. 5, the concentration $x = 0.3$ is a special case since then $n_{\text{tot}}^{\text{eff}} = 2$. The system is then effectively at half-filling and behaves as a Kondo insulator at large U , Δ^c , and low temperatures. The transition from a metal to a Kondo insulator at non-integer filling predicted here for the PAM [64] is a counterpart to the Mott-Hubbard metal-insulator transition at non-integral filling in the one-band Hubbard model discussed in [62,63].

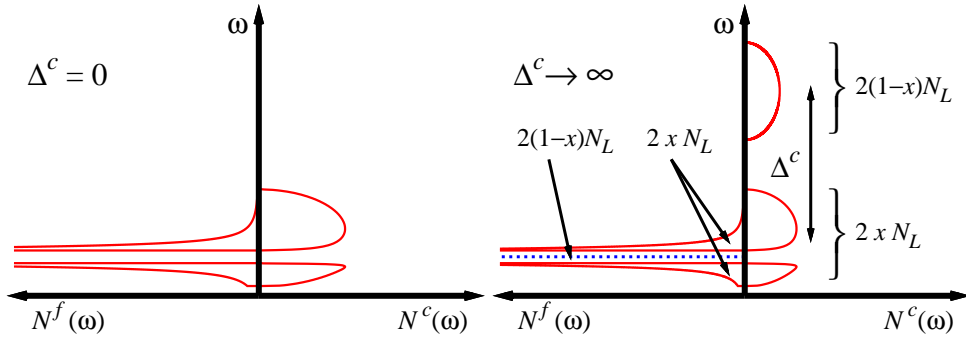


Fig. 4. Binary alloy splitting of the c - and f -electron density of states for $U = 0$. a) No disorder in the c -electron system ($\Delta^c = 0$). b) Limit of strong disorder, $\Delta^c \rightarrow \infty$; in this case $2(1-x)N_L$ non-dispersive f -electron states (dotted line) remain at ε^f and $2(1-x)N_L$ c -electron states are shifted to high energies.

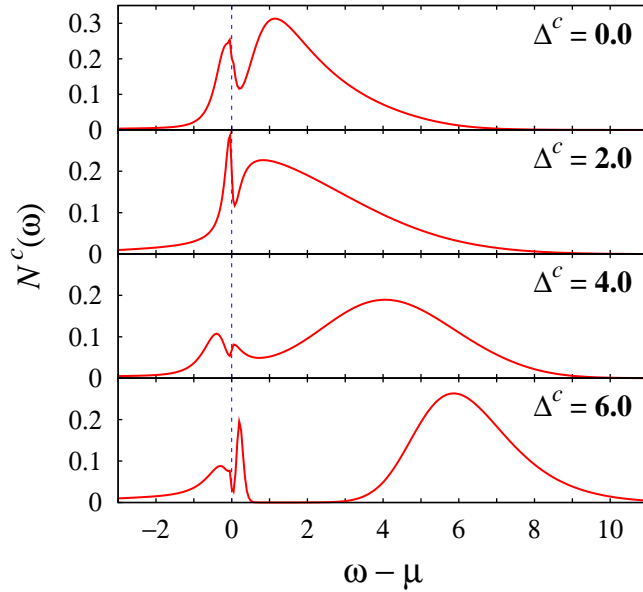


Fig. 5. Spectral function of c -electrons in the PAM for different Δ^c at $x = 0.3$ (other parameters: $U = 1.5$, $V = 0.5$, $\varepsilon_0^c - \varepsilon_0^f = 3.25$ and $n_{\text{tot}} = 1.3$) obtained within QMC and maximal entropy at $T = 1/60$. By increasing Δ^c a pseudogap opens, which becomes a real gap for $T \rightarrow 0$; after Ref. [64].

5.4 Disorder induced enhancement of the Curie temperature

It is well known that itinerant ferromagnetism occurs in the non-disordered Hubbard model (1) only off half-filling provided the DOS is asymmetric and peaked at the lower edge [65,66]. While the Curie temperature increases with the strength of the electron interaction one would expect it to be lowered by disorder. However, our investigations show that in some cases the Curie temperature can actually be increased by binary alloy disorder [62,67].

In the case of the PAM with binary alloy disorder we also found that under certain conditions the Curie temperature can actually be enhanced [64]. Indeed, as shown in the right panel of Fig. 6, the Curie temperature for the transition to the ferromagnetic state in the PAM is a non-monotonic function of the alloy concentration x . In particular, the behavior is quite different for disorder acting on the f - or the c -electrons.

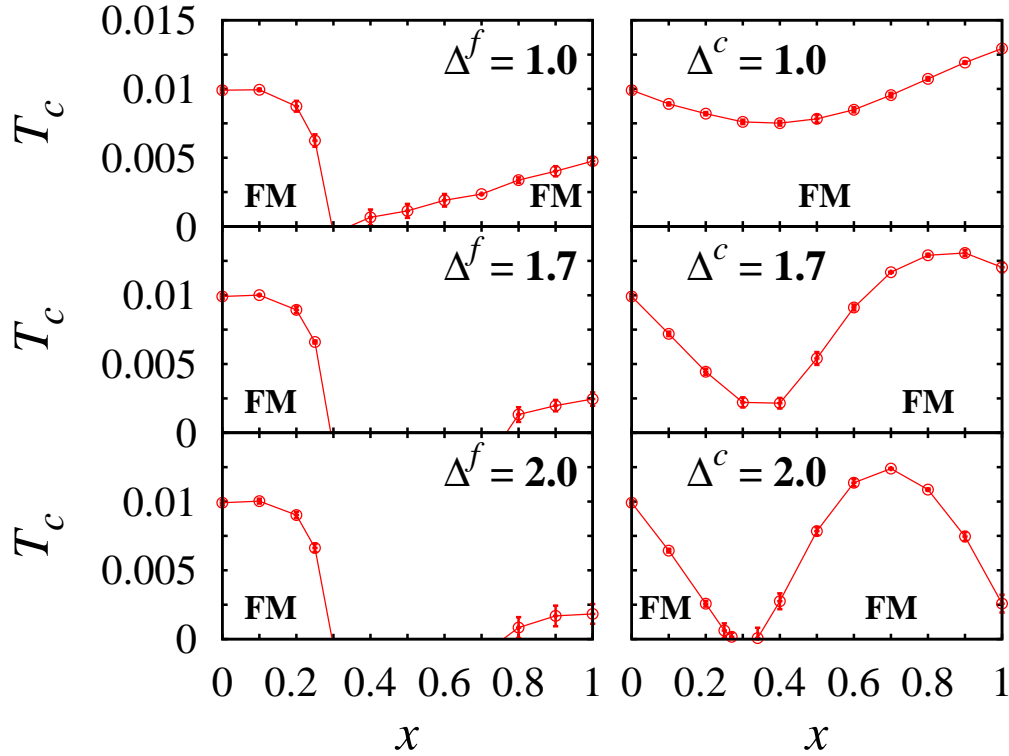


Fig. 6. Curie temperature in the PAM as a function of alloy concentration x and energy splitting Δ^f (left column) and Δ^c (right column) for $n_{\text{tot}} = 1.3$ and $\varepsilon_0^c - \varepsilon_0^f = 3.25$. Strong c -electron disorder enhances T_c compared to its values at $x = 0$ or 1 ; after Ref. [64].

5.4.1 f -electron disorder

As found by Meyer [68] the presence of f -electron disorder always reduces the Curie temperature relative to its non-disordered values at $x = 0$ or 1 . For strong enough disorder T_c eventually vanishes, e.g., at $x = 0.28$ and $x = 0.75$, respectively, for $\Delta^f = 1.7$ (right panel, left column of Fig. 6). This is due to the splitting of the f -electron band at large Δ^f which increases the double occupation of the lower alloy subband; this reduces the local moment of the f -electrons and thereby T_c .

5.4.2 c -electron disorder

Interestingly, c -electron disorder leads to a much more subtle dependence of T_c on concentration x . Namely, for increasing energy splitting Δ^c there are, in general, three different features observed, the physical origin of which will be discussed in more detail later:

- (i) at $x = 1$, i.e., in the non-disordered case, T_c is reduced,
- (ii) a minimum develops in T_c at $x = n_{\text{tot}} - 1 > 0$;
- (iii) T_c is *enhanced* over its non-disordered values at $x = 0$ or 1 . Altogether this leads to a global maximum in T_c vs. x . While the decrease of T_c at $x = 1$ is a simple consequence of the reduction of the energy difference between the f -level and the c -electron band, $\varepsilon^c - \varepsilon^f = \varepsilon_0^c - \varepsilon_0^f - \Delta^c$, for increasing Δ^c , the latter effects are more subtle.

5.4.3 Origin of the maximum in T_c

We will now explain the maximum in T_c vs. x . It can be understood within the following model based on an *ansatz* for the Curie temperature, $T_c(U, V, \mu) = T_c^0(U, V, \mu)F^c(\mu - \varepsilon_0^c)F^f(\mu - \varepsilon_0^f)$, which implies that the formation of local f -electron moments (F^f) is assumed to be independent from the c -electron mediated ordering of those moments (F^c). In fact, for the RKKY model this *ansatz* can be microscopically justified within a static mean-field theory. The two functions F^c , F^f are determined by T_c calculated within DMFT for the non-disorder case at fixed $\mu - \varepsilon_0^c$ or $\mu - \varepsilon_0^f$, respectively; they are shown in Fig. 7(a) and 7(b) for one set of parameters. The prefactor T_c^0 is determined by the requirement that the dimensionless functions F^f and F^c be equal to one at their maxima. We note that $F^f(\mu - \varepsilon_0^f)$ has a maximum when the f -level is half-filled ($\mu = \varepsilon_0^f + U/2$), i.e., when the local moment is maximal.

The Curie temperature in the presence of c -electron disorder can be estimated by averaging over the c -electron part, F^c , giving rise to the disorder-dependent function $\mathcal{F}^c(x, \mu - \varepsilon_0^c) = [xF^c(\mu - \varepsilon_0^c + \Delta^c) + (1 - x)F^c(\mu - \varepsilon_0^c)]$. The linear dependence on the alloy concentration can again be justified microscopically within a static mean-field theory for the RKKY model, where T_c depends linearly on the DOS at the chemical potential. T_c is now determined for each concentration x . We calculate μ , which is an implicit function of x , in the non-hybridized limit ($V = 0$) within a rigid band approximation. The dependence of the resulting functions $\mathcal{F}^c(x, \mu - \varepsilon_0^c)$ and $F^f(\mu - \varepsilon_0^f)$ on x are shown in Fig. 7(c) for $\Delta^c = 2.0$. In general $F^f(\mu - \varepsilon_0^f)$ has a global maximum at those values of x for which the f -level is half-filled [see Fig. 7(c)]. By contrast, $\mathcal{F}^c(x, \mu - \varepsilon_0^c)$ is characterized by a wide minimum, related to the formation of the pseudo-gap in the interacting DOS seen in Fig. 5. This minimum reaches zero, i.e., $\mathcal{F}^c(x, \mu - \varepsilon_0^c) = 0$, for a finite range of x values as shown in Fig. 7(c). The resulting $T_c(x)$ obtained by the product of these two functions agrees remarkably well with the numerical result obtained by DMFT as shown in Fig. 7(d).

5.5 Summary

In this paper we showed that the interplay between disorder and many-body correlations can lead to quite unexpected, often counter-intuitive, behavior. We first explored the low-temperature phases of the Anderson-Hubbard model within the dynamical mean-field theory in combination with a geometrical average over the disorder. This allows for a unified description of Anderson and Mott-localization on the basis of one-particle correlation functions. The paramagnetic phase diagram shows reentrant metal-insulator transitions caused by the interaction and disorder, and the Anderson and Mott insulating phases were found to be continuously connected. In the presence of antiferromagnetism a stabilizing effect of the simultaneous presence of interaction and disorder was discovered, which leads to a new antiferromagnetic metallic phase. An overall similar behavior concerning Anderson and Mott insulating phases is found in the Falicov-Kimball model. It is expected that the very interesting parameter regime of strong interactions and strong disorder, which is not easily accessible in correlated electron materials, can also be realized with cold atoms in optical lattices.

In a second application we investigated ferromagnetism and Kondo insulator behavior in the periodic Anderson model (PAM) in the presence of binary alloy disorder. Far away from half-filling the PAM shows ferromagnetic order. For strong enough binary alloy disorder the conduction band splits and the correlations among the f -electrons lead to a non-trivial dependence of the Curie temperature on the alloy concentration. Upon decreasing the alloy concentration the local moments increase which raises T_c , but at the same time the opening of a gap in the alloy Kondo insulator at non-integral filling leads to a decrease of T_c . In effect this causes the Curie temperature to behave non-monotonically as a function of the alloy concentration, with a global maximum in T_c which can be drastically larger than in the absence of disorder. The effect is predicted to occur in f -electron materials with alloy disorder in the conduction band, and also in ultracold fermionic atoms in optical lattices trapped by harmonic potentials in the presence of random binary disorder.

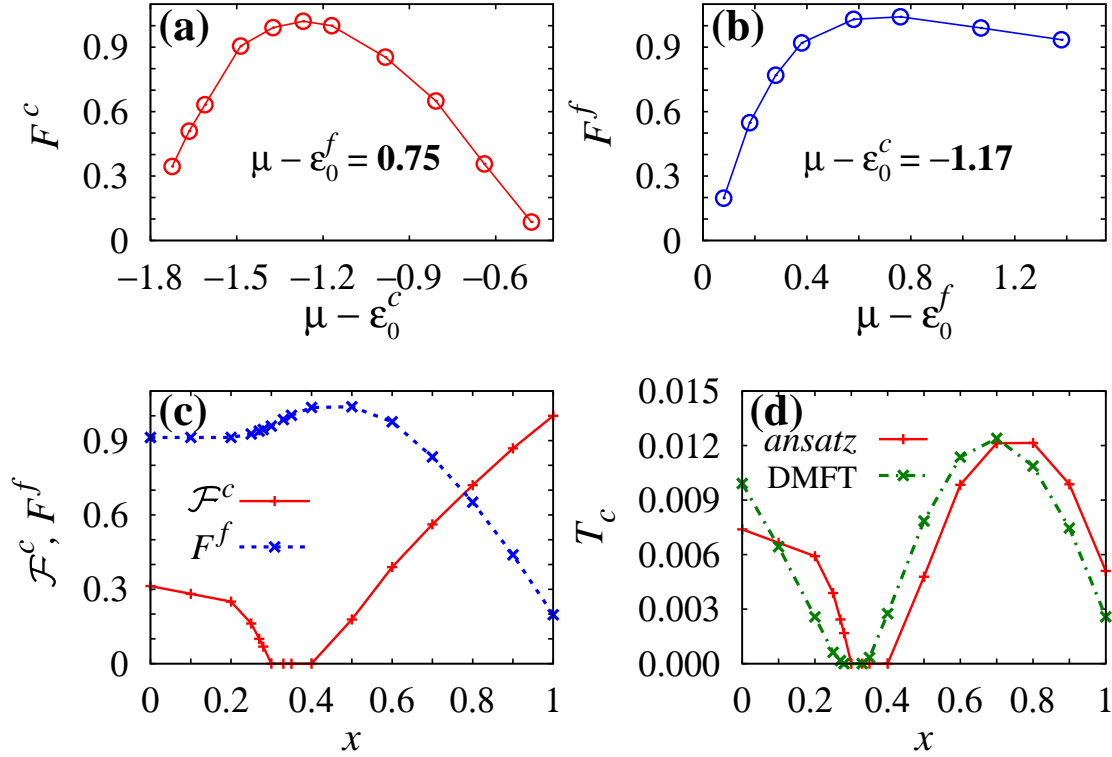


Fig. 7. (a) $F^c(\mu - \epsilon_0^c)$, (b) $F^f(\mu - \epsilon_0^f)$ appearing in the *ansatz* for T_c in the disordered PAM (see text) calculated for $\Delta^c = 0$. (c) $\mathcal{F}^c(\mu - \epsilon_0^c)$ and $F^f(\mu - \epsilon_0^f)$ for $\Delta^c = 2.0$; other parameters as in Fig. 6(b). (d) Comparison of T_c obtained from the *ansatz* and within DMFT; after Ref. [64].

We thank R. Bulla and S. Kehrein for useful discussions. Financial support by the SFB 484, TTR 80 and FOR 801 of the Deutsche Forschungsgemeinschaft is gratefully acknowledged.

References

1. J. H. de Boer, E. J. W. Verwey, Proc. Phys. Soc. **49**, No. 4S, 59 (1937)
2. N. F. Mott, Proc. Phys. Soc. **49**, No. 4S, 57 (1937)
3. D. Pines, *The Many-Body Problem* (W. A. Benjamin, Reading, 1962)
4. N. F. Mott, *Metal-Insulator Transitions* (Taylor and Francis, London, 1990)
5. P. Fulde, *Electron Correlations in Molecules and Solids* (Springer, Heidelberg, 1995)
6. M. Imada, A. Fujimori, Y. Tokura, Rev. Mod. Phys. **70**, 1039 (1998)
7. P. Fazekas, *Lecture Notes on Electron Correlation and Magnetism* (World Scientific, Singapore, 1999)
8. J. Spałek, Eur. J. Phys. **21**, 511 (2000)
9. P. W. Anderson, Phys. Rev. **109**, 1492 (1958)
10. P. A. Lee, T. V. Ramakrishnan, Rev. Mod. Phys. **57**, 287 (1985)
11. D. Vollhardt, P. Wölfle, in *Electronic Phase Transitions*, edited by W. Hanke, Y. V. KopaeV (North Holland, Amsterdam, 1992), p. 1
12. B. Kramer, A. Mac Kinnon, Rep. Prog. Phys. **56**, 1469 (1993)
13. F. Evers, A. D. Mirlin, Rev. Mod. Phys. **80**, 1355 (2008)
14. A. Lagendijk, B. van Tiggelen, D. S. Wiersma, Physics Today **62**, 24 (2009)
15. A. Aspect, M. Inguscio, Physics Today **62**, 30 (2009)
16. A. Richardella, P. Roushan, S. Mack, B. Zhou, D. A. Huse, D. D. Awschalom, A. Yazdani, Science **327**, 665 (2010)

17. L. Sanchez-Palencia, M. Lewenstein, *Nature Phys.* **6**, 87 (2010)
18. P. A. Lee, T. V. Ramakrishnan, *Rev. Mod. Phys.* **57**, 287 (1985)
19. D. Belitz and T. R. Kirkpatrick, *Rev. Mod. Phys.* **66**, 261 (1994)
20. S. V. Kravchenko, G. V. Kravchenko, J. E. Furneaux, V. M. Pudalov, M. D'Iorio, *Phys. Rev. B* **50**, 8039 (1994)
21. D. Popović, A. B. Fowler, S. Washburn, *Phys. Rev. Lett.* **79**, 1543 (1997)
22. S. V. Kravchenko and M. P. Sarachik, *Rep. Prog. Phys.* **67**, 1 (2004)
23. H. von Löhneysen, *Adv. in Solid State Phys.* **40**, 143 (2000)
24. A. M. Finkelshtein, *Sov. Phys. JEPT* **75**, 97 (1983)
25. C. Castellani, C. Di Castro, P. A. Lee, M. Ma, *Phys. Rev. B* **30**, 527 (1984)
26. M. A. Tusch, D. E. Logan, *Phys. Rev. B* **48**, 14843 (1993)
27. M. A. Tusch, D. E. Logan, *Phys. Rev. B* **51**, 11940 (1995)
28. D. L. Shepelyansky, *Phys. Rev. Lett.* **73**, 2607 (1994)
29. P. J. H. Denteneer, R. T. Scalettar, N. Trivedi, *Phys. Rev. Lett.* **87**, 146401 (2001)
30. D. Heidarian and N. Trivedi, *Phys. Rev. Lett.* **93** 126401 (2004)
31. N. F. Mott, *Proc. Phys. Soc. A* **62**, 416 (1949)
32. E. Abrahams, P. W. Anderson, D. C. Licciardello, T. V. Ramakrishnan, *Phys. Rev. Lett.* **42**, 673 (1979)
33. W. Metzner, D. Vollhardt, *Phys. Rev. Lett.* **62**, 324 (1989)
34. E. Müller-Hartmann, *Z. Phys. B* **76**, 211 (1989)
35. V. Janiš, *Z. Phys. B* **83**, 227 (1991)
36. V. Janiš, D. Vollhardt, *Int. J. Mod. Phys. B* **6**, 731 (1992)
37. A. Georges, G. Kotliar, *Phys. Rev. B* **45**, 6479 (1992)
38. M. Jarrell, *Phys. Rev. Lett.* **69**, 168 (1992)
39. D. Vollhardt, in *Correlated Electron Systems*, edited by V. J. Emery (World Scientific, Singapore, 1993), p. 57
40. Th. Pruschke, M. Jarrell, J. K. Freericks, *Adv. in Phys.* **44**, 187 (1995)
41. A. Georges, G. Kotliar, W. Krauth, M. J. Rozenberg, *Rev. Mod. Phys.* **68**, 13 (1996)
42. K. Held, I. A. Nekrasov, G. Keller, V. Eyert, N. Blümer, A. K. McMahan, R. T. Scalettar, Th. Pruschke, V. I. Anisimov, D. Vollhardt, *Psi-k Newsletter* **56**, 65 (2003); reprinted in *Phys. Status Solidi B* **243**, 2599 (2006)
43. G. Kotliar, D. Vollhardt, *Physics Today* **57**, No. 3 (March), 53 (2004)
44. G. Kotliar, S. Y. Savrasov, K. Haule, V. S. Oudovenko, O. Parcollet, C.A. Marianetti, *Rev. Mod. Phys.* **78**, 865 (2006)
45. J. K. Freericks, V. Zlatić, *Rev. Mod. Phys.* **75**, 1333 (2003)
46. J. K. Freericks, *Transport in multilayered nanostructures — The dynamical mean-field approach* (Imperial College Press, London, 2006)
47. K. Byczuk, W. Hofstetter, D. Vollhardt, *Phys. Rev. Lett.* **94**, 056404 (2005)
48. K. Byczuk, *Phys. Rev. B* **71**, 205105 (2005)
49. K. Byczuk, W. Hofstetter, D. Vollhardt, *Phys. Rev. Lett.* **102**, 146403 (2009)
50. D. Semmler, K. Byczuk, W. Hofstetter, *Phys. Rev. B* **81**, 115111 (2010)
51. V. Dobrosavljević, G. Kotliar, *Phys. Rev. Lett.* **78**, 3943 (1997)
52. V. Dobrosavljević, A. A. Pastor, B. K. Nikolić, *Europhys. Lett.* **62**, 76 (2003)
53. G. Schubert, A. Weiße, H. Fehske in *High Performance Computing in Science and Engineering Garching 2004*, edited by A. Bode, F. Durst (Springer, Heidelberg, 2005), p. 237
54. G. Schubert, J. Schleede, K. Byczuk, H. Fehske, and D. Vollhardt, arXiv:1002.2895
55. M. Ulmke, V. Janiš, D. Vollhardt, *Phys. Rev. B* **51**, 10411 (1995)
56. K. G. Wilson, *Rev. Mod. Phys.* **47**, 773 (1975)
57. W. Hofstetter, *Phys. Rev. Lett.* **85**, 1508 (2000)
58. R. Bulla, Th. Costi, T. Pruschke, *Rev. Mod. Phys.* **80**, 395 (2008)
59. Th. Pruschke, *Prog. Theo. Phys. Suppl.* **160**, 274 (2005)
60. A. Singh, M. Ulmke, D. Vollhardt, *Phys. Rev. B* **58**, 8683 (1998)
61. R. Bulla, M. Potthoff, *Eur. Phys. J. B* **13**, 257 (2000)
62. K. Byczuk, M. Ulmke, D. Vollhardt, *Phys. Rev. Lett.* **90**, 196403 (2003)
63. K. Byczuk, W. Hofstetter, D. Vollhardt, *Phys. Rev. B* **69**, 045112 (2004)
64. U. Yu, K. Byczuk, D. Vollhardt, *Phys. Rev. Lett.* **100**, 246401 (2008)
65. M. Ulmke, *Eur. Phys. J. B* **1**, 301 (1998)
66. J. Wahle, N. Blümer, J. Schlipf, K. Held, D. Vollhardt, *Phys. Rev. B* **58**, 12749 (1998)
67. K. Byczuk, M. Ulmke, *Eur. Phys. J. B* **45**, 449-454 (2005)
68. D. Meyer, *Solid State Commun.* **121**, 565 (2002)